ACS Photonics

Open Access

pubs.acs.org/journal/apchd5

Article

Robust Isolated Attosecond Pulse Generation with Self-Compressed Subcycle Drivers from Hollow Capillary Fibers

Marina Fernández Galán,* Javier Serrano, Enrique Conejero Jarque, Rocío Borrego-Varillas, Matteo Lucchini, Maurizio Reduzzi, Mauro Nisoli, Christian Brahms, John C. Travers, Carlos Hernández-García, and Julio San Roman

Cite This: *ACS Photonics* 2024, 11, 1673−1683

Read Online

ACCESS | Metrics & More | Article Recommendations

ABSTRACT: High-order harmonic generation (HHG) arising from the nonperturbative interaction of intense light fields with matter constitutes a well-established tabletop source of coherent extreme-ultraviolet and soft X-ray radiation, which is typically emitted as attosecond pulse trains. However, ultrafast applications increasingly demand isolated attosecond pulses (IAPs), which offer great promise for advancing precision control of electron dynamics. Yet, the direct generation of IAPs typically requires the synthesis of near-single-cycle intense driving fields, which is technologically challenging. In this work, we theoretically demonstrate a novel scheme for the straightforward and compact generation of IAPs from multicycle infrared drivers using hollow capillary fibers (HCFs). Starting from a standard, intense multicycle infrared pulse, a light transient is generated by extreme soliton self-compression in a HCF with decreasing pressure and is subsequently used to drive HHG in a gas target. Owing to the subcycle confinement of the HHG process, high-contrast IAPs are continuously emitted almost independently of the carrier-envelope phase (CEP) of the optimally self-compressed drivers. This results in a CEP-robust scheme which is also stable under macroscopic propagation of the high harmonics in a gas target. Our results open the way to a new generation of integrated all-fiber IAP sources, overcoming the efficiency limitations of usual gating techniques for multicycle drivers.

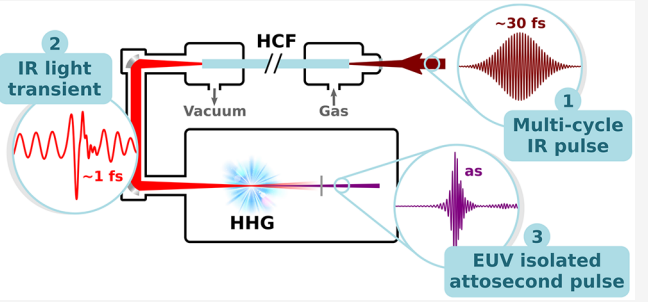

KEYWORDS: *nonlinear optics, ultrashort laser pulses, soliton self-compression, hollow capillary fibers, high-order harmonic generation, isolated attosecond pulses*

1. INTRODUCTION

Laser sources delivering broadband ultrashort pulses are of paramount importance for ultrafast science. In a continuous effort to access the briefest phenomena in nature, the temporal resolution afforded by this technology has advanced through 12 orders of magnitude in the last five decades, overcoming the ultimate limit set by the period of the carrier wave. In the last years, the generation of subcycle optical waveforms has enabled unprecedented control of electron dynamics and strong field processes.[1,2] Among the latter, high harmonic generation (HHG) stands out as the only tabletop process capable of providing coherent extreme-ultraviolet (EUV) and soft X-ray radiation.[3] In the semiclassical microscopic picture of HHG in gaseous media,[4] an intense infrared (IR) laser pulse first tunnel-ionizes the atoms and coherently drives the motion of the free electrons. Second, after reversal of the driving electric field, the electrons are driven back to the parent ions and, upon recollision, high frequency radiation is emitted. As the entire HHG process is repeated every half cycle of the IR pulse, standard high harmonic emission consists of a train of attosecond bursts.[5,6] This unique ultrafast source has opened the door to time-resolved studies of valence electron motion in atoms[7,8] or charge migration in molecules,[9−11] among many others.[12,13] Nevertheless, for certain applications, the isolation of a single attosecond pulse from the train is preferred. For this purpose, different gating techniques have been developed, allowing for the generation of isolated attosecond pulses (IAPs) from commercially available multicycle IR pulses. These consist on controlling the rescattering process on the microscopic level like polarization gating[14−16] or two-color and double optical gating,[17−19] taking advantage of macroscopic propagation effects like ionization gating or time-gated phase-matching,[20−25] or implementing the attosecond lighthouse effect based on spatiotemporal wavefront control.[26,27]

Received: December 22, 2023
Revised: March 5, 2024
Accepted: March 5, 2024
Published: March 18, 2024

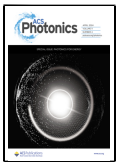

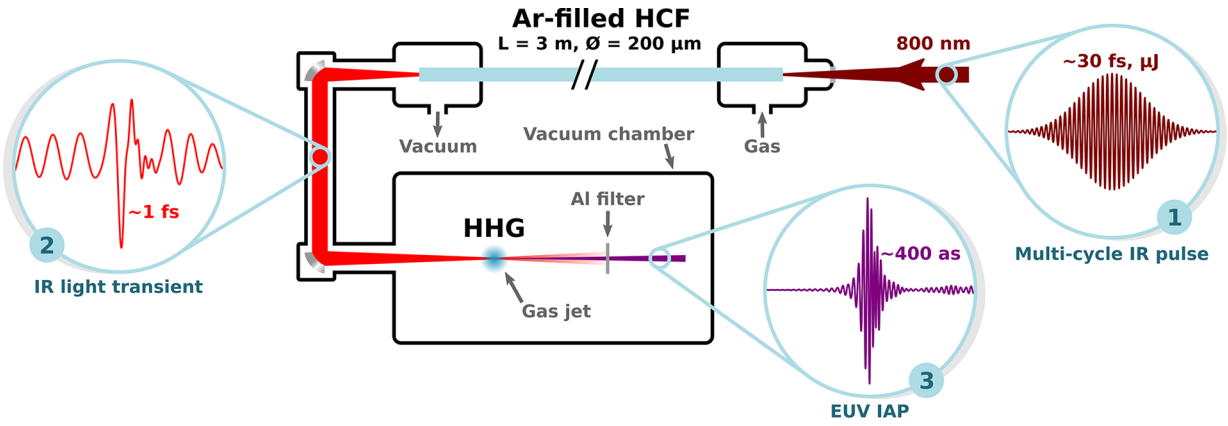

Figure 1. Schematic of an in-vacuum HHG beamline driven by subcycle self-compressed pulses from a gas-filled HCF with a decreasing pressure gradient. Starting from a multicycle IR pulse (1), a light transient (2) is generated by extreme soliton self-compression in the fiber and subsequently used to produce EUV IAPs (3) in a gas target.

Simpler techniques, like amplitude gating with few-cycle drivers, have also been demonstrated,[28,29] but these require an additional spectral selection of the high-energy cutoff produced by the most intense half cycle of the driving field, precluding the generation of ultrabroadband IAPs.[30] Since the first experimental confirmation of amplitude gating in 2001,[31] this technique has been refined to overcome this bandwidth limitation by the use of ever shorter IR pulses down into the subcycle regime. These waveforms naturally confine the HHG process to the only intense half cycle of the electric field, and recently, precise tailoring of driving transients has allowed the direct creation of highly tunable IAPs and enhanced HHG spectra.[32−34] However, the subcycle control of light transients often requires the use of extremely complex systems, like the so-called parametric waveform synthesizers.[35] Therefore, next-generation HHG experiments would strongly benefit from the availability of more compact and handy sources of subcycle optical drivers.

A very promising alternative for the generation of subcycle IR pulses comes through high-energy soliton dynamics in gas-filled hollow capillary fibers (HCFs).[36] These simple fibers are routinely used for ultrashort pulse compression[37] and allow for significant energy scaling and nonlinearity and dispersion tuning by modifying the pressure of the filling gas.[38] In particular, if the latter is chosen so that an input multicycle pulse propagates in the HCF with anomalous dispersion, the simultaneous nonlinear spectral broadening by self-phase modulation (SPM) and phase compensation arising from the negative group-velocity dispersion (GVD) can lead to soliton self-compression well down into the subcycle regime.[39,40] Recent studies have demonstrated that this extreme pulse compression can be further enhanced by pumping the fiber with a decreasing pressure gradient[41] and that broadly similar high-quality subcycle IR fields can be generated in different HCF scenarios.[42] In addition, the use of decreasing pressure could be of great interest for HHG experiments, as it allows for the direct delivery to vacuum of the self-compressed pulses free of distortions from transmission optics.[43,44] Altogether, the combination of HHG beamlines with HCFs delivering intense self-compressed IR transients opens a very promising scenario to develop compact and versatile scientific tools for the generation of high-frequency IAPs, but theoretical investigations and design guidelines are still missing to make it a feasible technique.

In this work, we demonstrate a unique control in the efficient generation of IAPs from self-compressed multicycle IR pulses, combining for the first time in a compact scheme the advantages of using state-of-the-art femtosecond pump pulses with the possibilities offered by subcycle waveform tailoring. We numerically study HHG driven by IR subcycle pulses generated by extreme soliton self-compression in a gas-filled HCF with a decreasing pressure gradient that allows direct delivery to a vacuum beamline. By systematically scanning the energy of the input pulse to the fiber, its output carrier-envelope phase (CEP) and the pumping gas pressure, different IR fields are synthesized. When driving HHG with these unique waveforms, we can control the properties of the generated high-order harmonics and attosecond pulses. In particular, our results demonstrate that high-contrast IAPs are directly produced for a broad set of driving fields corresponding to the optimally self-compressed IR pulses. Most interestingly, owing to the nature of the IR waveforms, clean IAPs are continuously emitted for a wide range of driver CEPs, resulting in a CEP-robust scheme which is also stable under macroscopic propagation of the high harmonics in a gas target. Our results open the door to a new generation of HCF-based IAP sources for ultrafast applications and also provide a compact tool to explore the role of isolated attosecond pulses in recent works of quantum HHG.[45,46]

2. METHODS

Figure 1 shows the proposed scheme comprising a first stage of pulse self-compression in a gas-filled HCF and subsequent HHG in a gas target driven by the subcycle waveforms exiting the fiber. The capillary is negatively pumped, i.e., filled with a decreasing pressure gradient, with the gas supplied at the entrance at a pressure p_0, and the output end directly coupled to the vacuum beamline at pressure $p_L = 0$. In this way, the resulting pressure distribution along the longitudinal coordinate z of the fiber is given by[47]

$$p(z) = \sqrt{p_0^2 + \frac{z}{L}(p_L^2 - p_0^2)} = p_0\sqrt{1 - \frac{z}{L}} \quad (1)$$

where L represents the HCF length. The first fiber stage is theoretically modeled with a (2 + 1)D multimode nonlinear propagation equation for the pulse complex envelope $\mathcal{E}(\rho, T, z)$, which can be written as

https://doi.org/10.1021/acsphotonics.3c01897
ACS Photonics 2024, 11, 1673−1683

$$\frac{\partial}{\partial z}\mathcal{E}(\rho, T, z) = (\hat{L} + \hat{N}[\mathcal{E}(\rho, T, z)])\mathcal{E}(\rho, T, z) \quad (2)$$

where the operator $\hat{L}$ accounts for the linear propagation effects of diffraction, complete chromatic dispersion and linear losses, and $\hat{N}$ includes the nonlinear effects of self-phase modulation (SPM), self-steepening, and photoionization and plasma absorption. A detailed description of each term and their mathematical form can be found in refs 48 and 49. Here the pulse propagation equation is expressed in a local time $T = t - z/v_g$ measured in a reference frame traveling with the pulse at the group velocity v_g, and the spatial pulse envelope is assumed to have cylindrical symmetry and depend only upon the radial coordinate $\rho = \sqrt{x^2 + y^2}$.

Equation 2 is numerically solved with a standard split-step Fourier method,[50] where each propagation step Δz is divided into two substeps. In the first substep, linear effects alone are applied by decomposing $\mathcal{E}(\rho, T, z)$ into the linearly polarized EH_{1m} modes of the HCF and advancing each mode with its complex propagation constant $\beta_m(\omega)$:[51]

$$\mathcal{E}'(\rho, \omega, z + \Delta z) = \sum_{m=1}^{\infty} c_m(\omega, z) EH_{1m}(\rho) \exp\{i\beta_m(\omega)\Delta z\} \quad (3)$$

where ω stands for angular frequency and $\mathcal{E}'(\rho, \omega, z + \Delta z)$ is the direct Fourier transform of $\mathcal{E}(\rho, T, z + \Delta z)$. The coefficients $c_m(\omega, z)$ of the modal expansion are computed with an inverse Hankel transform of the spatial beam distribution in the fiber core, and up to 30 modes are typically considered in the simulations. In the second substep, the nonlinearity is assumed to act alone, and eq 2 with $\hat{L} = 0$ is integrated in the time domain with a fourth-order Runge–Kutta algorithm. In addition, to first explore different self-compression scenarios and perform systematic parameter scans, we reduce the (2 + 1)D computationally demanding model to a time-dependent (1 + 1)D nonlinear propagation equation for the fundamental EH_{11} mode of the HCF, neglecting spatial and plasma dynamics.[41,49] This approximation accurately describes ultrashort pulse propagation in the low-intensity regime, where the peak power and the peak intensity of the pulse remain, respectively, below the critical power for self-focusing and the threshold intensity for gas ionization.[52]

When complete (2 + 1)D simulations are performed, the cylindrically symmetric pulse at the HCF output $\mathcal{E}(\rho, T, z)$ is then propagated in vacuum and focused onto a low density gas target to drive HHG, as depicted in Figure 1. The beam free-space expansion from z to $z + \Delta z$ is numerically accomplished by expressing $\mathcal{E}(\rho, T, z)$ as a superposition of plane monochromatic waves and multiplying each Fourier component by its corresponding propagation phase:[53]

$$\tilde{\mathcal{E}}(k_\rho, \omega, z) = \int_0^\infty \rho \mathcal{E}'(\rho, \omega, z) J_0(k_\rho \rho)\, \mathrm{d}\rho \quad (4)$$

$$\tilde{\mathcal{E}}(k_\rho, \omega, z + \Delta z) = \tilde{\mathcal{E}}(k_\rho, \omega, z) \exp\left\{i\Delta z\left(k_z(\omega) - k_{z,0} - \frac{\omega - \omega_0}{v_{g,0}}\right)\right\} \quad (5)$$

where k_ρ and k_z are radial and axial wave numbers, $\tilde{\mathcal{E}}(k_\rho, \omega, z)$ is the Hankel transform of $\mathcal{E}'(\rho, \omega, z)$, and $J_0(x)$ is the zeroth order Bessel function of the first kind. The dispersion relation in vacuum is given by $k_z^2 = \omega^2/c^2 - k_\rho^2$, where c is the speed of light, $k_{z,0} = k_z(\omega = \omega_0, k_\rho = 0) = \omega_0/c$ is the wavenumber of a plane wave at the central frequency ω_0 propagating in the longitudinal direction, and $v_{g,0} = v_g(\omega = \omega_0, k_\rho = 0) = c$ is the speed of a reference frame moving with the group velocity of the pulse, with $v_g = (\partial k_z/\partial\omega)^{-1}$. After its free-expansion, the beam is focused with an ideal concave mirror, which is modeled in the frequency domain as a quadratic spatial phase $\sim \exp\{-i\omega\rho^2/(2cf)\}$, f being its focal length. This procedure recovers a perfect image of the HCF output at the focal plane,[54] with a suitable intensity for driving efficient HHG.

The corresponding IR electric field around the focal volume is generated by adding the carrier wave as $E_0(\rho, T, z) = \Re[\mathcal{E}(\rho, T, z)\exp\{-i\omega_0 T + i\phi_{CEP}\}]$, ϕ_{CEP} being the CEP, and it is used as input to macroscopic HHG calculations in a gas target. Note that, as $\mathcal{E}(\rho, T, z)$ is a complex quantity with its own temporal phase, $\phi_{CEP} = 0$ might not correspond to the situation of maximum field amplitude. In the HHG simulations, the generation medium is discretized into elementary radiators and single-atom harmonic contributions are computed through the full integration of the three-dimensional time-dependent Schrödinger equation (3D-TDSE), under the single-active electron approximation, which is given by

$$i\hbar\frac{\partial}{\partial T}\Psi(\mathbf{r}, T) = \frac{1}{2m_e}\left(-i\hbar\nabla + \frac{e}{c}\mathbf{A}_j(T)\right)^2 \Psi(\mathbf{r}, T) + V_C(\mathbf{r})\Psi(\mathbf{r}, T) \quad (6)$$

where $\Psi(\mathbf{r}, T)$ is the electronic wave function, m_e is the electron mass, $e = |e|$ is the elementary charge, $V_C(\mathbf{r})$ is the Coulomb potential, and $\mathbf{A}_j(T)$ is the vector potential associated with the linearly polarized driving field at the atom position $\mathbf{r}_j$, i.e., $\mathbf{E}_0(\mathbf{r}_j, T) = -(1/c)(\partial/\partial T)\mathbf{A}_j(T)$. Equation 6 is solved using the Crank–Nicolson finite difference method and the dipole acceleration $\mathbf{a}_j(T)$ of the jth charge is obtained from the mean value of the operator $-(1/m_e)\nabla V_C(\mathbf{r})$.

The emissions from each accelerated charge in the target are then propagated to a far-field detector through the electromagnetic field propagator, thus taking into account the phase-matching of the high-order harmonics. The transversal far-field radiated by the charge at $\mathbf{r}_j$ is given by[55]

$$\mathbf{E}_j(\mathbf{r}_d, T) = -\frac{e}{c^2|\mathbf{r}_d - \mathbf{r}_j|}\mathbf{s}_d \times (\mathbf{s}_d \times \mathbf{a}_j[T - |\mathbf{r}_d - \mathbf{r}_j|/c]) \quad (7)$$

where $\mathbf{s}_d = \mathbf{r}_d/|\mathbf{r}_d|$ is a unitary vector pointing to a virtual detector located at $\mathbf{r}_d$, and $\mathbf{a}_j$ is evaluated at the retarded time. Under the dipole approximation, the charge displacement during the interaction is considered small in comparison to the wavelength of the driving field and, thus, the position $\mathbf{r}_j$ in eq 7 is assumed to be time-independent. Finally, the elementary fields are coherently added in the detector to obtain the total emission:

$$\mathbf{E}(\mathbf{r}_d, T) = \mathbf{E}_0(\mathbf{r}_d, T) + \sum_{j=1}^{n} \mathbf{E}_j(\mathbf{r}_d, T) \quad (8)$$

The number of atoms n considered in the simulations is large enough to reach the convergence of the results. The fundamental and low-order harmonics are last filtered with a 200 nm-thick aluminum foil. Note that we considered that, after the HCF, the IR driving field propagates in vacuum, neglecting dispersion and nonlinear reshaping in the gas jet, an

https://doi.org/10.1021/acsphotonics.3c01897
ACS Photonics 2024, 11, 1673−1683

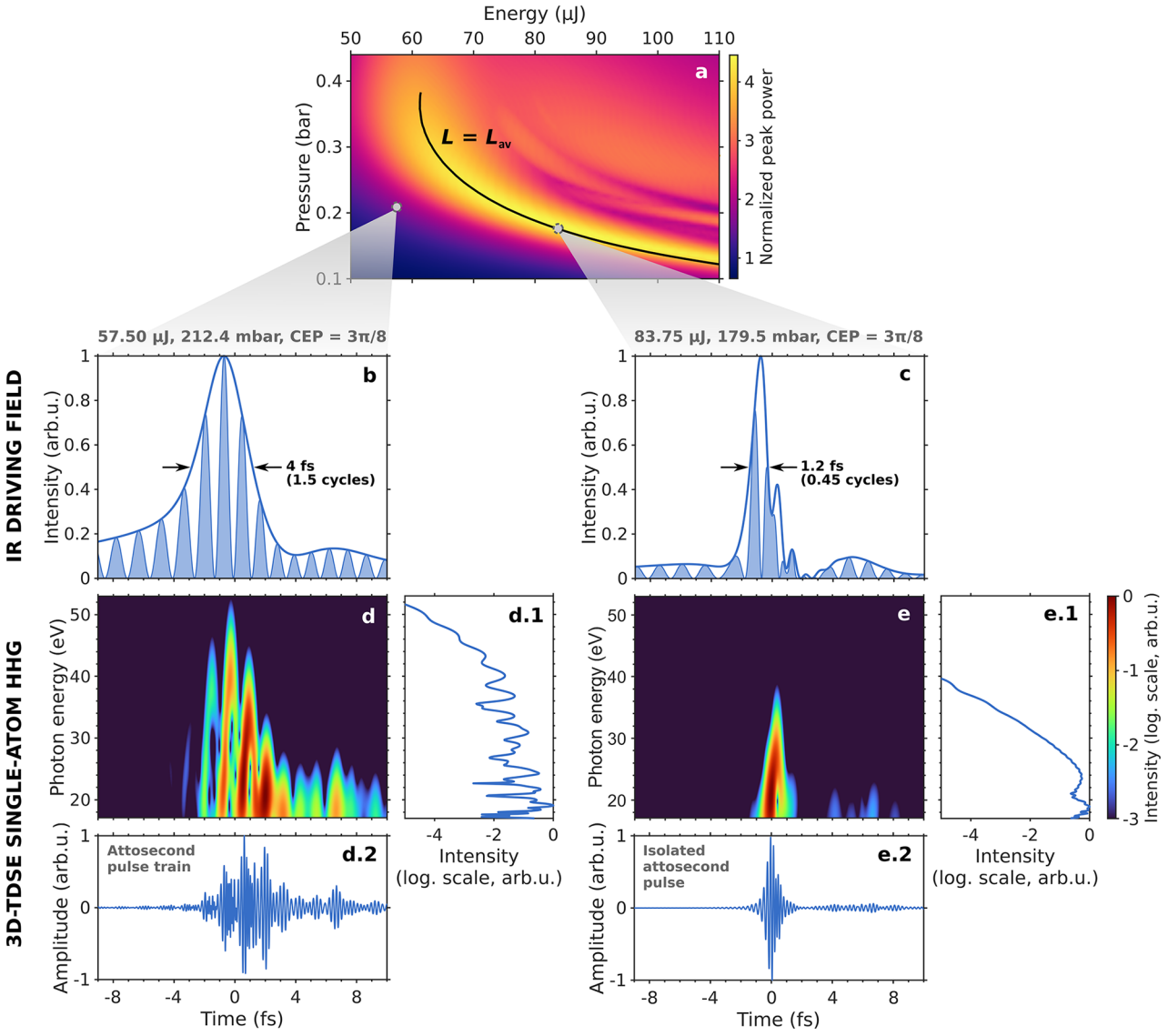

Figure 2. (a) Ratio of output to input peak power of the self-compressed IR pulses as a function of the initial energy U_0 and the equivalent constant pressure p_{eq} in the negatively pumped 100 μm core-radius, 3 m long HCF filled with Ar. The solid black line represents the contour where $L = L_{av}$, which runs along the optimal region for subcycle self-compression. (b, c) Self-compressed IR drivers generated in the HCF for two different sets of (U_0, p_{eq}, ϕ_{CEP}): (b) a few-cycle pulse and (c) a subcycle light transient. (d, e) Time-frequency analysis of their corresponding single-atom HHG emissions in hydrogen when their instantaneous peak intensity is set to 1.57×10^{14} W/cm^2 (electric field amplitude of 0.067 au). Additional panels (d.1, e.1) show the high-harmonic spectra and (d.2, e.2) their temporal counterpart in the form of an attosecond pulse train or a clean IAP.

assumption that is valid in the case of moderate pulse intensities and low density targets (~10^{17} atoms/cm^3) such as those used in standard HHG experiments.[55]

3. RESULTS AND DISCUSSION

3.1. Optimal Subcycle Self-Compression and HHG Regimes. First, to produce a wide variety of ultrashort IR waveforms and investigate their influence on HHG, we have followed the procedure detailed in ref.[41] In short, using the (1 + 1)D propagation model, we have simulated the self-compression of a 30 fs (intensity full width at half-maximum, fwhm) transform-limited Gaussian pulse at 800 nm through a 3 m long, 100 μm core-radius HCF filled with argon, while varying its initial energy U_0 and the equivalent pressure p_{eq}. The latter is defined as the constant gas pressure which matches the nonlinear phase-shift acquired by the pulse during its propagation through the negatively pumped fiber and, for a pressure distribution in the form of eq 1, it is simply related to the pumping pressure by $p_{eq} = 2p_0/3$.[44]

For each (U_0, p_{eq}) pair, Figure 2a shows the ratio of output to input peak power of the self-compressed pulses. In this plot, the optimal region for high-quality subcycle pulse generation can be readily identified as the area of largest peak power enhancement, which was also found to overlap with the region of shortest output pulse duration.[41,42] In the decreasing pressure configuration, this optimal self-compression region is in general delimited by two constraints. On one hand, the soliton order must be kept $N < 15$ to achieve a high-quality compression without triggering modulation instabilities.[56,57] On the other hand, the fixed fiber length has to match the characteristic length of the process to ensure that the self-compressing pulse reaches the minimum possible duration without entering in the soliton fission regime. In previous works, an average self-compression length was defined as[41]

https://doi.org/10.1021/acsphotonics.3c01897
ACS Photonics 2024, 11, 1673−1683

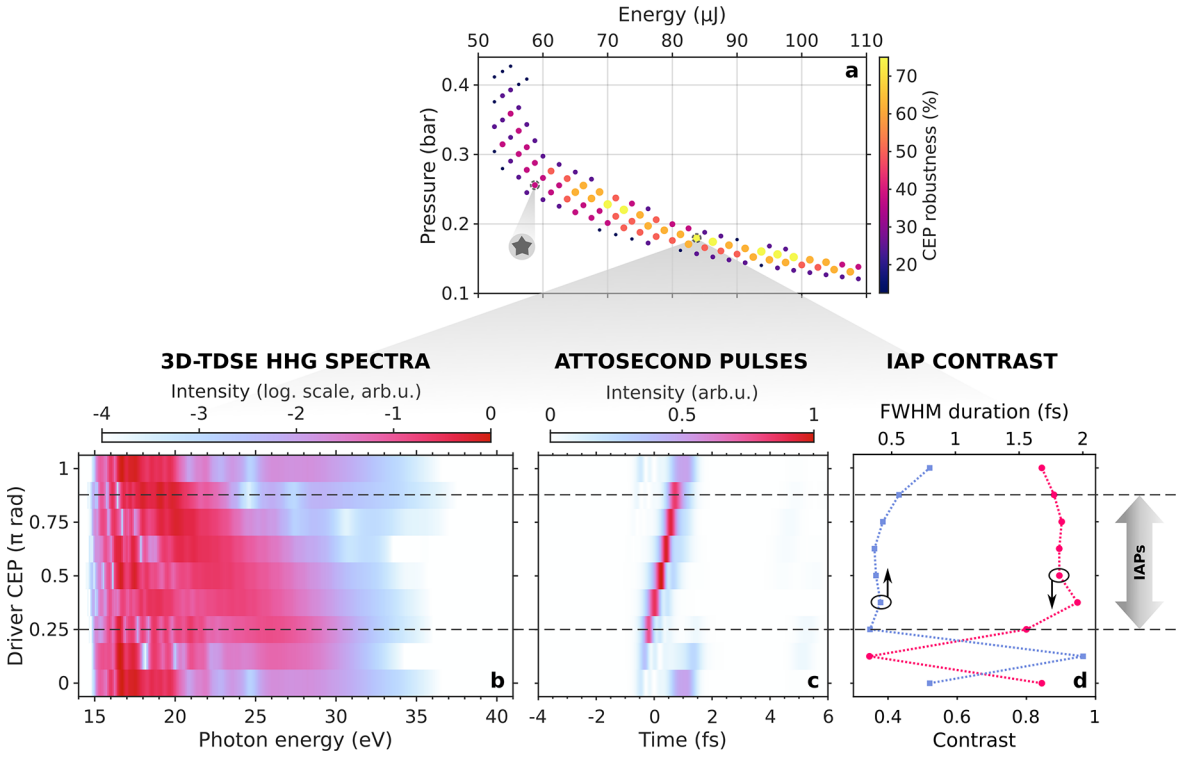

Figure 3. (a) Robustness of the IAPs to variations in the CEP of the subcycle drivers which are generated in the HCF for different pairs of pump energy and gas pressure. The highlighted point with a star label refers to the situation shown in Figure 4. (b) Single-atom HHG spectra as a function of the CEP of the IR driving field generated in the HCF for an input pulse energy U_0 = 83.75 μJ and an equivalent Ar pressure p_{eq} = 179.5 mbar. (c) Temporal profile and (d) fwhm intensity duration and contrast of the corresponding attosecond pulses.

$$L_{av} = \frac{L_{sc} + L_{fiss}}{2} = \frac{1+\sqrt{2}}{2\sqrt{2}} L_{fiss} \tag{9}$$

where $L_{fiss} = L_D/N$ is the fission length,[57] $L_{sc} = L_{fiss}/\sqrt{2}$ is a self-compression length,[58] $N = (L_D/L_{NL})^{1/2}$ is the soliton order, and $L_D = T_p^2/(4 \ln 2|\beta_2|)$ and $L_{NL} = 1/(\gamma P_0)$ determine the characteristic length scales of GVD and SPM, respectively.[50] Here T_p represents the fwhm duration of the input Gaussian pulse, P_0 refers to its peak power, β_2 is the GVD coefficient of the HCF, and γ is the nonlinear parameter as defined elsewhere.[50] As also shown in Figure 2a, the condition $L = L_{av}$ describes a contour line in the energy-pressure plane which, when falling inside the space with $N < 15$, can be used to identify the optimal region for high-quality self-compression in any configuration.[42]

After simulating the first HCF stage, we have generated different IR fields from each self-compressed pulse by adding the carrier wave with eight values of ϕ_{CEP} ranging from 0 to π rad. We verified with a carrier-resolved propagation code that, in our range, this can be equally accomplished by varying the CEP of the input pulse, which is a more realistic experimental scenario. However, from the computational point of view, we found it more efficient for the parameter sweeps to propagate the pulse envelope and then build the electric field at the HHG generation points. The resulting large set of waveforms, each identified by (U_0, p_{eq}, ϕ_{CEP}), was used to perform single-atom 3D-TDSE HHG calculations in atomic hydrogen. This target species was chosen for simplicity, but the 3D-TDSE could be easily extended to other noble gases (Ar, He, Kr, Ne), under the single-active electron approximation. In addition, to isolate the influence of the driving waveform itself in HHG, all IR drivers were first normalized to an instantaneous peak intensity of 1.57 × 10^{14} W/cm^2 (corresponding to an electric field amplitude of 0.067 atomic units, au). Experimentally, this could be achieved by inserting a variable attenuator in the beam path in Figure 1 or by adjusting the focusing geometry. Finally, the temporal and spectral properties of the harmonic radiation (maximum photon energy, isolation of attosecond pulses, contrast, etc.) were analyzed in terms of the free parameters (U_0, p_{eq}, ϕ_{CEP}), providing useful design guidelines for experiments.

Two representative examples of HHG driven by IR self-compressed pulses are shown in Figures 2b–e. In the region below the contour line $L = L_{av}$, the propagating pulse exits the fiber before reaching the maximum self-compression point, resulting in driving fields with few-cycle durations like the one shown in Figure 2b. The results of the 3D-TDSE HHG calculations for this IR pulse are shown in the time-frequency analysis (also known as spectrogram) in Figure 2d, which encodes the complete information on the HHG emission both in intensity and phase. As we can see in Figure 2d.2, this kind of suboptimal self-compressed pulses yield attosecond pulse trains in the temporal domain, but their HHG spectra (Figure 2d.1) were found to reach the highest photon energies because the field strength is preserved after the ionization HHG step with longer pulses.

As the product $U_0 \times p_{eq}$ is increased, the output pulses from the HCF become shorter until high-quality subcycle waveforms are generated in the region around the contour $L = L_{av}$. Figure 2c shows one of such IR light transients, which reached an intensity fwhm duration of 1.2 fs corresponding to 0.45 optical cycles at the initial central wavelength of 800 nm. The single-atom HHG spectrum for this driving waveform is shown

https://doi.org/10.1021/acsphotonics.3c01897
ACS Photonics 2024, 11, 1673−1683

in Figure 2e.1 and visibly presents a lower cutoff energy than the spectrum corresponding to the previous 4 fs pulse. This is because the time-integrated electric field strength after the ionization step (i.e., the energy accumulated by the free electrons during their acceleration in the laser field) is smaller for the subcycle than for the few-cycle pulse. In addition, as we can see from the complete time-frequency analysis in Figure 2e, these subcycle IR fields tightly constrict the whole HHG process, with all the harmonics being emitted in a very narrow temporal window, leading to the direct generation of clean IAPs (see Figure 2e.2). Note that, despite their subcycle nature, the temporal duration of all the studied waveforms was found to be still sufficient to allow for the recombination HHG step to occur.

3.2. Robustness of IAP Generation against the CEP of Subcycle Drivers. We now focus on the situations where the self-compressed pulses from the HCF directly lead to the emission of high-order harmonics in the form of clean IAPs. In Figure 3a, we plot all the investigated (U_0, p_{eq}) pairs that produced IAPs. For a systematic search, we considered an attosecond pulse to be isolated whenever the intensity of the secondary temporal bursts remained below 10% of the peak intensity. As we can clearly realize by comparing Figures 2a and 3a, the region for IAP generation matches the region for optimal subcycle self-compression in the HCF running along the contour line $L = L_{av}$.

For these ultrashort IR driving waveforms, the intensity envelope $|\mathcal{E}(\rho, z, T)|^2$ evolves in the same temporal scale as the carrier oscillations. Therefore, the CEP becomes of critical importance in the HHG process as it determines the particular variation of the laser electric field in time. Being driven by the electromagnetic field itself, all effects in strong-field laser interactions have demonstrated to be sensitive to the CEP,[59,60] and HHG is no exception. In particular, attosecond pulse production has been found to be very sensitive to the driver CEP when working with few-cycle pulses. In this regime, known as the nonadiabatic regime, CEP variations leave a clear imprint in the high-harmonic spectra due to the interference between consecutive attosecond bursts,[7,61−64] and adequate values of CEP can even lead to the generation of IAPs if the resulting electric field limits the emission of harmonics to a single recollision event. As a consequence, one would expect a similar or stronger dependence on the CEP for our self-compressed subcycle pulses.

To gain insight into these effects, we have first computed the robustness of the generated IAPs to variations in their driver CEP for each point in Figure 3a. This parameter is represented both in the color scale and with the markers size. For the subcycle pulse envelope generated in the HCF for each point (U_0, p_{eq}), we defined the CEP robustness as the percentage of values of $\phi_{CEP} \in [0, \pi]$ for which the resulting electric fields lead to the direct emission of IAPs according to the aforementioned isolation criterion. Noticeably, many cases exhibit very high values of CEP robustness around 50−60%, the best cases reaching up to 75%.

In addition, the complete 3D-TDSE HHG simulations results for an optimal case with 75% of CEP robustness are shown in Figure 3b−d. From left to right, the three columns depict (b) the HHG spectra, (c) the corresponding temporal profile, and (d) the fwhm duration and contrast of the attosecond pulses generated with each subcycle IR driver as a function of its CEP. Here, contrast is defined as the ratio of energy within the main attosecond pulse to the overall energy transmitted through the aluminum filter. As we can see, clean IAPs are continuously generated in most of the CEP range. In all cases, these IAPs exhibit a great contrast above 0.8 and a fwhm duration of around 350−450 as. In the frequency domain, the generation of IAPs is accompanied by a smooth cutoff free of spectral fringes. Changes in the CEP of the driving field shift the recollision time along the pulse envelope,[64] resulting in a temporal drift of the attosecond pulses as clearly seen in Figure 3c. Despite these variations in emission times, HHG spectra and IAP durations, the most outstanding feature is that the single attosecond pulse isolation is preserved for most of the CEP range. This is presumably because, for optimally self-compressed IR drivers, the subcycle duration of the intensity envelope always limits the HHG process to a single recollision event from the only intense half cycle.

For those few cases where a second attosecond burst starts to show, the contrast drops abruptly and deep interference modulations appear in the harmonic spectra. It is also interesting to point out that these deteriorated cases appear around $\phi_{CEP} = 0$, and not only the attosecond pulse is not isolated, but also the total yield is very low. This can be understood from the fact that two consecutive driving electric field peaks are involved in the HHG process, respectively for the ionization and recombination steps. In subcycle waveforms with CEP $\sim$ 0, which consist of a main peak surrounded by low-intensity structure, either the ionizing or recombinating field amplitude is weak, resulting in a low harmonic signal. On the contrary, subcycle drivers with intermediate values of CEP present two consecutive peaks with similar field strength and thus yield the brightest IAPs. Therefore, subcycle pulses with $\phi_{CEP} = 0$ appear not to be the ideal drivers for HHG, and we expect even shorter pulses with these CEP values to prevent any EUV emission due to the absence of returning field to drive the free electrons back to the parent ion.[2]

3.3. IAP Robustness against Macroscopic HHG. Previous results for the whole set of IR waveforms were obtained from single-atom 3D-TDSE calculations, already providing a general insight into the properties of HHG driven by self-compressed pulses from HCFs. However, being a highly nonlinear process, the amplitude and phase of the harmonic emission is very sensitive to the details of the driving field. As a result, a complete description of HHG should include propagation and phase-matching of the harmonics in the gas target.[21,55,65−69] In particular, for ultrabroadband subcycle waveforms, diffraction-induced spatiotemporal reshaping and changes in the CEP of the driving pulse around the focal volume can affect the efficient buildup of the harmonics emitted across the target and hinder the isolation of clean attosecond pulses.

To analyze the impact of macroscopic propagation in the generation of IAPs, we have performed a complete HHG simulation in a gas jet for $U_0 = 58.75\ \mu J$ and $p_{eq} = 255.8$ mbar. According to the single-atom calculations, this situation presented a low CEP robustness of ∼37%, as shown in Figure 3a with the star label. This relatively sensitive case was chosen to study the influence of propagation, because we expect the optimal cases presenting higher CEP robustness to be less affected by phase-matching. Using these input parameters, we computed the (2 + 1)D self-compression of the pump pulse in the HCF. Although the output on-axis temporal profile was found to be almost identical to the one previously obtained from the (1 + 1)D model, the (2 + 1)D simulation provided

https://doi.org/10.1021/acsphotonics.3c01897
ACS Photonics 2024, 11, 1673−1683

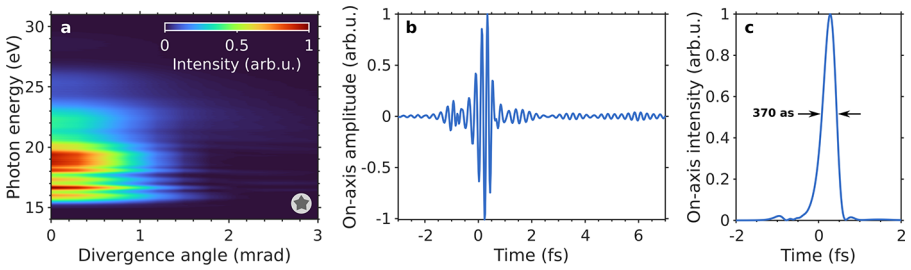

Figure 4. (a) Harmonic spectrum as a function of the divergence angle in the far-field detector obtained by driving the HHG process, in a 1 mm thick low-density hydrogen jet centered at the beam focus, with the subcycle IR pulse obtained from the HCF for U_0 = 58.75 μJ, p_{eq} = 255.8 mbar, and $\phi_{CEP} = 5\pi/8$ rad (corresponding to the situation labeled in Figure 3a with a star) and focused and attenuated to an instantaneous peak intensity of 1.82 × 10^{14} W/cm^2 (field amplitude of 0.072 au). (b) Resulting on-axis attosecond pulse and (c) its temporal intensity profile.

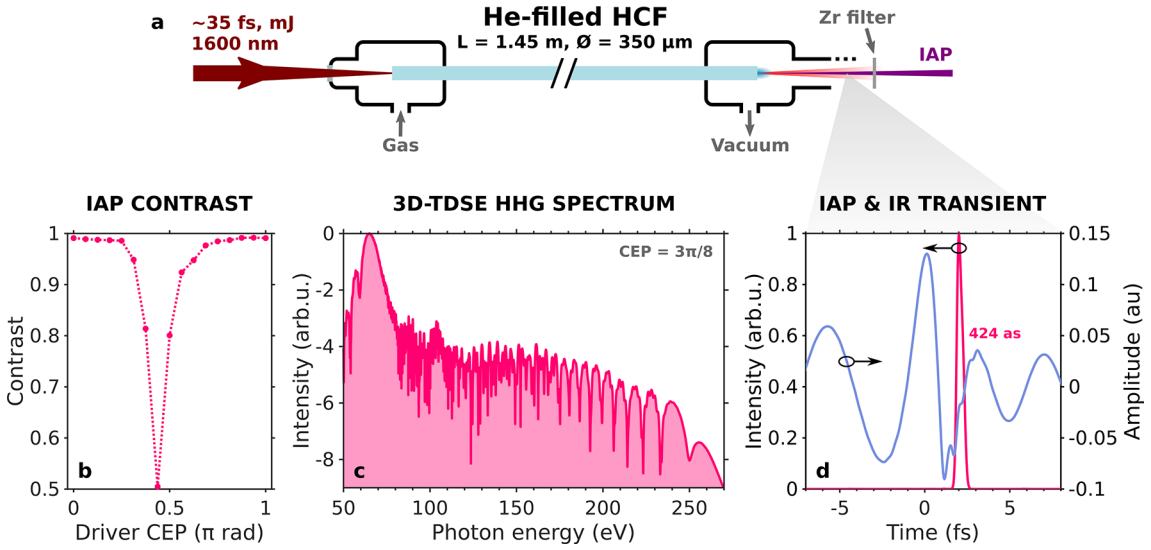

Figure 5. (a) Schematic of an all-fiber IAP source, where HHG is directly driven at the HCF end by a self-compressed, high-energy IR subcycle transient. (b) Contrast of the directly emitted IAPs as a function of the CEP of the driving 2.2 fs, 1.3 mJ self-compressed pulse at 1600 nm, generated in the helium-filled HCF. (c) Single-atom 3D-TDSE high-harmonic spectrum in He for the waveform with $\phi_{CEP} = 3\pi/8$ rad, after transmission through a zirconium filter. (d) Corresponding IAP (fuchsia line) plotted over the main feature of the IR driving field.

the real spatial profile at the fiber end. This beam was then freely propagated in vacuum along a distance of 1 m and subsequently focused with one spherical mirror (f = 30 cm) to a spot radius of approximately 30 μm, corresponding to a Rayleigh length $z_R \sim$ 3.5 mm at 800 nm. The driving waveform was built with $\phi_{CEP} = 5\pi/8$ rad, as this yielded the cleanest IAP in the single-atom simulations, and attenuated to an instantaneous peak intensity of 1.82 × 10^{14} W/cm^2 to avoid barrier suppression. The complete IR pulse around the focal volume was finally used as input for macroscopic HHG calculations in a 1 mm thick, low-density hydrogen jet centered at the beam focus. Figure 4a shows the resulting harmonic spectrum as a function of the divergence angle in the far-field detector, after spatial integration along the azimuthal coordinate. All harmonics are emitted with a low divergence <1 mrad, and a highly contrasted 370-as IAP is generated across the whole EUV beam. Its on-axis temporal amplitude and intensity profile are shown in Figure 4b,c. This is in good agreement with the predictions of the single-atom 3D-TDSE calculations, and we expect the optimal cases exhibiting the highest CEP robustness to also tolerate phase-matching effects, as further confirmed by additional macroscopic simulations in longitudinal and transversal targets not shown here. These results demonstrate that the proposed scheme is indeed capable of generating high-quality IAPs which remain stable upon CEP variations and phase-matching in a gas target. Although it is out of the scope of this paper, further macroscopic HHG optimization by controlling beam size, wavefront curvature, and gas jet pressure and relative position to beam focus, could be additionally used to modify the IAP properties, such as pulse duration, chirp or divergence.[65,68−72]

3.4. High-Energy Subcycle Self-Compression toward an All-Fiber IAP Source. Given the discussion above on IAP generation following extreme pulse self-compression in a single HCF step, it is natural to ask whether the scheme presented in Figure 1 could be further simplified by removing the focusing stage and generating high-order harmonics directly at the fiber end, as shown in Figure 5a. All-fiber HHG sources have been briefly envisioned both theoretically and experimentally in hollow-core photonic crystal fibers,[57,73,74] and a compact soft X-ray source, enabled by self-compression of ∼2 μm pulses in an antiresonant HCF, has been recently demonstrated.[75] Nevertheless, to the best of our knowledge, this scenario has not yet been explored in simpler and larger-core HCFs, where high intensities can be routinely reached. In these systems, achieving a sufficiently high intensity at the fiber output so as to directly drive efficient HHG would require pumping with millijoule-level pulses and carefully choosing a relatively small core radius to boost the peak intensity without causing unaffordable losses. However, at high intensities, ionization

https://doi.org/10.1021/acsphotonics.3c01897
ACS Photonics 2024, 11, 1673−1683

might also become a problem, both because it leads to severe distortion of the self-compressing pulse and because it complicates the phase-matching of the harmonics due to strong free-electron dispersion. Furthermore, as a high energy pulse self-compresses toward subcycle durations, its peak power drastically increases, which can lead to beam self-focusing and additional gas ionization if the peak power exceeds the critical value P_{cr}.[76] Fortunately, as both ionization and P_{cr} scale inversely with the gas density, these detrimental nonlinear effects can be ameliorated with the decreasing pressure gradient configuration.

As a proof of concept of an all-fiber IAP source, we have followed the scaling rules presented before to translate subcycle self-compression to millijoule-level pulses which could directly drive HHG at the fiber end. One immediately realizes that, to achieve a high-quality compression, the constraint $N < 15$ inevitably sets an upper limit to the maximum pump energy. By further inspection of the soliton order, it is straightforward to prove that, in a first approximation where only the waveguide dispersion is considered, $N \propto (p_{eq} T_p U_0/\lambda_0^4)^{1/2}$. As a result, if N is to take some optimal value below 15, then $U_0 \propto N^2\lambda_0^4/(p_{eq}T_p)$ and, thus, the most efficient way to upscale the pulse energy is to increase the initial central wavelength λ_0 by moving toward the mid-IR spectral region. The combination of higher energies and longer wavelengths would definitely be of great interest for HHG experiments. Indeed, short-wavelength- and mid-IR drivers have been widely used to achieve high photon energies up to the soft X-rays.[3,77−79] Now, thanks to a stronger HCF anomalous response at longer wavelengths, this energy scaling can be accomplished even in more practical fibers ($L \sim 1$ m).

As an example of this scaling principle, we have used the complete (2 + 1)D model to simulate the self-compression of an input 2-mJ, 35 fs Gaussian pulse centered at 1600 nm through a 1.45 m long, 175 μm core radius, helium-filled HCF with a decreasing pressure gradient from $p_0 = 3.15$ bar to $p_L = 0.15$ bar. In this case, He was chosen to avoid problems with ionization and the fiber end was left with some pressure instead of completely evacuated so that the HHG generation medium could be the filling gas itself. Nevertheless, we verified with the simulations that the output pressure p_L could be approximately varied in the range from 0 to 0.3 bar without incurring any noticeable distortions to the self-compressed driver. This fact could give some freedom to adjust the phase-matching of the high-harmonics. In the configuration with $p_L = 0.15$ bar, the IR pulse self-compresses to an output subcycle duration of 2.2 fs, corresponding to 0.41 optical cycles at 1600 nm, and retains 1.3 mJ of energy. This yields a peak intensity of 7.2×10^{14} W/cm^2 at the fiber end, or a peak power of 0.2 TW when integrating over the spatial profile, which is high enough to directly drive HHG in He.

After adding the carrier wave with different values of ϕ_{CEP}, the resulting waveforms were used to perform single-atom 3D-TDSE HHG calculations in He. Note that full macroscopic HHG simulations at this longer IR wavelength using the 3D-TDSE are beyond the state-of-the-art computational capabilities: first because the nonadiabatic nature of the subcycle pulses precludes the use of faster algorithms like those relying on the strong-field approximation and instead requires the use of the full-quantum 3D-TDSE,[80] and second because its numerical integration becomes very demanding already at the microscopic level, with high photon energies requiring a small time step and long wavelengths requiring a large spatial grid to fit the electron trajectories. Here, as opposed to previous simulations, the driving electric fields were directly used with the amplitude corresponding to the 1.3 mJ pulse at the HCF end for each CEP, without applying any normalization. Reaching higher photon energies in He than in hydrogen, the HHG spectra were now filtered with a 200 nm thick zirconium foil. As we can see in Figure 5b, this configuration also yields IAPs with a very high contrast approaching unity for more than half of the complete CEP range. For instance, Figure 5c shows the broadband HHG spectrum generated by the waveform with $\phi_{CEP} = 3\pi/8$ rad, which in the temporal domain yields the clean IAP plotted in Figure 5d over the main feature of the corresponding IR subcycle field.

4. CONCLUSIONS

In conclusion, we have theoretically demonstrated a compact and robust scheme for generating EUV IAPs from high-order harmonics. Starting from a standard multicycle IR pulse, a light transient is generated by extreme soliton self-compression in a negatively pumped HCF, and is subsequently used to drive HHG in a gas target leading to the direct emission of IAPs without the need for additional gating techniques. Systematic nonlinear pulse propagation simulations combined with full-quantum 3D-TDSE HHG calculations have shown that high-contrast IAPs are directly emitted for a broad set of driving fields corresponding to the optimally self-compressed IR pulses. This provides a general route toward robust IAP generation for any HCF configuration, since the pump energy and gas pressure which lead to optimal subcycle pulse compression, and thus to IAP emission, can be identified in a universal manner by matching the fiber length to an average self-compression length. Most remarkably, owing to the nature of the IR waveforms, the single attosecond pulse isolation is preserved for most of the driver CEPs, presumably because the subcycle duration of the intensity envelope continuously constricts the HHG process to a single recollision event from the only intense half cycle of the electric field. In addition to being CEP robust, the proposed scheme has also shown to be stable under macroscopic propagation including phase-matching of the high-order harmonics in a low-density gas target. Finally, we have provided preliminary theoretical advice for the development of all-fiber IAP sources driven by self-compressed millijoule-level subcycle IR pulses. Altogether, we believe that these findings might pave the way toward a new generation of compact and robust experiments for IAP generation with subcycle drivers, which, among other applications, offer great promise for advancing real-time observation and precision control of electron dynamics at the atomic scale.

AUTHOR INFORMATION

Corresponding Author

Marina Fernández Galán − *Grupo de Investigación en Aplicaciones del Láser y Fotónica, Departamento de Física Aplicada, Universidad de Salamanca, Salamanca 37008, Spain; Unidad de Excelencia en Luz y Materia Estructuradas (LUMES), Universidad de Salamanca, Salamanca 37008, Spain;* orcid.org/0000-0003-3047-1244; Email: marinafergal@usal.es

https://doi.org/10.1021/acsphotonics.3c01897
ACS Photonics 2024, 11, 1673−1683

Authors

Javier Serrano − *Grupo de Investigación en Aplicaciones del Láser y Fotónica, Departamento de Física Aplicada, Universidad de Salamanca, Salamanca 37008, Spain; Unidad de Excelencia en Luz y Materia Estructuradas (LUMES), Universidad de Salamanca, Salamanca 37008, Spain;* orcid.org/0000-0003-2093-2000

Enrique Conejero Jarque − *Grupo de Investigación en Aplicaciones del Láser y Fotónica, Departamento de Física Aplicada, Universidad de Salamanca, Salamanca 37008, Spain; Unidad de Excelencia en Luz y Materia Estructuradas (LUMES), Universidad de Salamanca, Salamanca 37008, Spain;* orcid.org/0000-0002-5328-6714

Rocío Borrego-Varillas − *Institute for Photonics and Nanotechnologies (IFN), Consiglio Nazionale delle Ricerche (CNR), Milano 20133, Italy*

Matteo Lucchini − *Institute for Photonics and Nanotechnologies (IFN), Consiglio Nazionale delle Ricerche (CNR), Milano 20133, Italy; Department of Physics, Politecnico di Milano, Milano 20133, Italy;* orcid.org/0000-0001-6476-100X

Maurizio Reduzzi − *Institute for Photonics and Nanotechnologies (IFN), Consiglio Nazionale delle Ricerche (CNR), Milano 20133, Italy; Department of Physics, Politecnico di Milano, Milano 20133, Italy*

Mauro Nisoli − *Institute for Photonics and Nanotechnologies (IFN), Consiglio Nazionale delle Ricerche (CNR), Milano 20133, Italy; Department of Physics, Politecnico di Milano, Milano 20133, Italy;* orcid.org/0000-0003-2309-732X

Christian Brahms − *School of Engineering and Physical Sciences, Heriot-Watt University, Edinburgh EH14 4AS, United Kingdom*

John C. Travers − *School of Engineering and Physical Sciences, Heriot-Watt University, Edinburgh EH14 4AS, United Kingdom*

Carlos Hernández-García − *Grupo de Investigación en Aplicaciones del Láser y Fotónica, Departamento de Física Aplicada, Universidad de Salamanca, Salamanca 37008, Spain; Unidad de Excelencia en Luz y Materia Estructuradas (LUMES), Universidad de Salamanca, Salamanca 37008, Spain;* orcid.org/0000-0002-6153-2647

Julio San Roman − *Grupo de Investigación en Aplicaciones del Láser y Fotónica, Departamento de Física Aplicada, Universidad de Salamanca, Salamanca 37008, Spain; Unidad de Excelencia en Luz y Materia Estructuradas (LUMES), Universidad de Salamanca, Salamanca 37008, Spain;* orcid.org/0000-0002-2645-7039

Complete contact information is available at: https://pubs.acs.org/10.1021/acsphotonics.3c01897

Funding

Ministerio de Ciencia e Innovación, Agencia Estatal de Investigación (PID2022-142340NB-I00); European Research Council (851201, 951224); and Ministerio de Universidades (FPU21/02916).

Notes

The authors declare no competing financial interest.

■ ACKNOWLEDGMENTS

This project has received funding from Ministerio de Ciencia e Innovación (MCIN/AEI/10.13 039/501100011033, I+D+i Grant PID2022-142340NB-I00) and from the European Research Council (ERC) under the European Union's Horizon 2020 Research and Innovation Program (Grant Agreement Nos. 851201 and 951224). M.F.G. acknowledges support from Ministerio de Universidades under Grant FPU21/02916. The authors thankfully acknowledge RES resources provided by BSC in MareNostrum 4, and SCAYLE in Caléndula to RES-FI-2022-3-0041.

■ REFERENCES

(1) Wirth, A.; Hassan, M. T.; Grguraš, I.; Gagnon, J.; Moulet, A.; Luu, T. T.; Pabst, S.; Santra, R.; Alahmed, Z. A.; Azzeer, A. M.; Yakovlev, V. S.; Pervak, V.; Krausz, F.; Goulielmakis, E. Synthesized light transients. *Science* **2011**, *334*, 195−200.

(2) Hassan, M. T.; Luu, T. T.; Moulet, A.; Raskazovskaya, O.; Zhokhov, P.; Garg, M.; Karpowicz, N.; Zheltikov, A. M.; Pervak, V.; Krausz, F.; Goulielmakis, E. Optical attosecond pulses and tracking the nonlinear response of bound electrons. *Nature* **2016**, *530*, 66−70.

(3) Popmintchev, T.; et al. Bright coherent ultrahigh harmonics in the keV X-ray regime from mid-infrared femtosecond lasers. *Science* **2012**, *336*, 1287−1291.

(4) Schafer, K. J.; Yang, B.; Dimauro, L. F.; Kulander, K. C. Above threshold ionization beyond the high harmonic cutoff. *Phys. Rev. Lett.* **1993**, *70*, 1599−1602.

(5) Farkas, G.; Tóth, C. Proposal for attosecond light pulse generation using laser induced multiple-harmonic conversion processes in rare gases. *Phys. Lett. A* **1992**, *168*, 447−450.

(6) Paul, P.-M.; Toma, E. S.; Breger, P.; Mullot, G.; Augé, F.; Balcou, P.; Muller, H. G.; Agostini, P. Observation of a train of attosecond pulses from high harmonic generation. *Science* **2001**, *292*, 1689−1692.

(7) Baltuška, A.; Udem, T.; Uiberacker, M.; Hentschel, M.; Goulielmakis, E.; Gohle, C.; Holzwarth, R.; Yakovlev, V. S.; Scrinzi, A.; Hänsch, T. W.; Krausz, F. Attosecond control of electronic processes by intense light fields. *Nature* **2003**, *421*, 611−615.

(8) Goulielmakis, E.; Loh, Z.-H.; Wirth, A.; Santra, R.; Rohringer, N.; Yakovlev, V. S.; Zherebtsov, S.; Pfeifer, T.; Azzeer, A. M.; Kling, M. F.; Leone, S. R.; Krausz, F. Real-time observation of valence electron motion. *Nature* **2010**, *466*, 739−743.

(9) Calegari, F.; Ayuso, D.; Trabattoni, A.; Belshaw, L.; De Camillis, S.; Anumula, S.; Frassetto, F.; Poletto, L.; Palacios, A.; Decleva, P.; Greenwood, J. B.; Martín, F.; Nisoli, M. Ultrafast electron dynamics in phenylalanine initiated by attosecond pulses. *Science* **2014**, *346*, 336−339.

(10) Kraus, P. M.; Mignolet, B.; Baykusheva, D.; Rupenyan, A.; Horný, L.; Penka, E. F.; Grassi, G.; Tolstikhin, O. I.; Schneider, J.; Jensen, F.; Madsen, L. B.; Bandrauk, A. D.; Remacle, F.; Wörner, H. J. Measurement and laser control of attosecond charge migration in ionized iodoacetylene. *Science* **2015**, *350*, 790−795.

(11) Nisoli, M.; Decleva, P.; Calegari, F.; Palacios, A.; Martín, F. Attosecond electron dynamics in molecules. *Chem. Rev.* **2017**, *117*, 10760−10825.

(12) Shi, X.; Liao, C.-T.; Tao, Z.; Cating-Subramanian, E.; Murnane, M. M.; Hernández-García, C.; Kapteyn, H. C. Attosecond light science and its application for probing quantum materials. *J. Phys. B* **2020**, *53*, 184008.

(13) Borrego-Varillas, R.; Lucchini, M.; Nisoli, M. Attosecond spectroscopy for the investigation of ultrafast dynamics in atomic, molecular and solid-state physics. *Rep. Prog. Phys.* **2022**, *85*, 066401.

(14) Sansone, G.; Benedetti, E.; Calegari, F.; Vozzi, C.; Avaldi, L.; Flammini, R.; Poletto, L.; Villoresi, P.; Altucci, C.; Velotta, R.; Stagira, S.; De Silvestri, S.; Nisoli, M. Isolated single-cycle attosecond pulses. *Science* **2006**, *314*, 443−446.

(15) Sola, I. J.; Mével, E.; Elouga, L.; Constant, E.; Strelkov, V.; Poletto, L.; Villoresi, P.; Benedetti, E.; Caumes, J. P.; Stagira, S.; Vozzi, C.; Sansone, G.; Nisoli, M. Controlling attosecond electron dynamics by phase-stabilized polarization gating. *Nat. Phys.* **2006**, *2*, 319−322.

(16) Sansone, G.; Ferrari, F.; Vozzi, C.; Calegari, F.; Stagira, S.; Nisoli, M. Towards atomic unit pulse duration by polarization-controlled few-cycle pulses. *J. Phys. B* **2009**, *42*, 134005.
(17) Mashiko, H.; Gilbertson, S.; Li, C.; Khan, S. D.; Shakya, M. M.; Moon, E.; Chang, Z. Double optical gating of high-order harmonic generation with carrier-envelope phase stabilized lasers. *Phys. Rev. Lett.* **2008**, *100*, 103906.
(18) Takahashi, E. J.; Lan, P.; Mücke, O. D.; Nabekawa, Y.; Midorikawa, K. Infrared two-color multicycle laser field synthesis for generating an intense attosecond pulse. *Phys. Rev. Lett.* **2010**, *104*, 233901.
(19) Zhao, K.; Zhang, Q.; Chini, M.; Wu, Y.; Wang, X.; Chang, Z. Tailoring a 67 attosecond pulse through advantageous phase-mismatch. *Opt. Lett.* **2012**, *37*, 3891−3893.
(20) Sandhu, A. S.; Gagnon, E.; Paul, A.; Thomann, I.; Lytle, A.; Keep, T.; Murnane, M. M.; Kapteyn, H. C.; Christov, I. P. Generation of sub-optical-cycle, carrier-envelope-phase-insensitive, extreme-UV pulses via nonlinear stabilization in a waveguide. *Phys. Rev. A* **2006**, *74*, 061803.
(21) Popmintchev, T.; Chen, M.-C.; Bahabad, A.; Gerrity, M.; Sidorenko, P.; Cohen, O.; Christov, I. P.; Murnane, M. M.; Kapteyn, H. C. Phase matching of high harmonic generation in the soft and hard X-ray regions of the spectrum. *Proc. Natl. Acad. Sci. U.S.A.* **2009**, *106*, 10516−10521.
(22) Thomann, I.; Bahabad, A.; Liu, X.; Trebino, R.; Murnane, M. M.; Kapteyn, H. C. Characterizing isolated attosecond pulses from hollow-core waveguides using multi-cycle driving pulses. *Opt. Express* **2009**, *17*, 4611−4633.
(23) Ferrari, F.; Calegari, F.; Lucchini, M.; Vozzi, C.; Stagira, S.; Sansone, G.; Nisoli, M. High-energy isolated attosecond pulses generated by above-saturation few-cycle fields. *Nat. Photonics* **2010**, *4*, 875−879.
(24) Chen, M.-C.; Mancuso, C.; Hernández-García, C.; Dollar, F.; Galloway, B.; Popmintchev, D.; Huang, P.-C.; Walker, B.; Plaja, L.; Jarón-Becker, A. A.; Becker, A.; Murnane, M. M.; Kapteyn, H. C.; Popmintchev, T. Generation of bright isolated attosecond soft X-ray pulses driven by multicycle midinfrared lasers. *Proc. Natl. Acad. Sci. U.S.A.* **2014**, *111*, E2361−E2367.
(25) Hernández-García, C.; Popmintchev, T.; Murnane, M. M.; Kapteyn, H. C.; Plaja, L.; Becker, A.; Jaron-Becker, A. Isolated broadband attosecond pulse generation with near- and mid-infrared driver pulses via time-gated phase matching. *Opt. Express* **2017**, *25*, 11855−11866.
(26) Vincenti, H.; Quéré, F. Attosecond lighthouses: how to use spatiotemporally coupled light fields to generate isolated attosecond pulses. *Phys. Rev. Lett.* **2012**, *108*, 113904.
(27) Kim, K. T.; Zhang, C.; Ruchon, T.; Hergott, J.-F.; Auguste, T.; Villeneuve, D.; Corkum, P.; Quéré, F. Photonic streaking of attosecond pulse trains. *Nat. Photonics* **2013**, *7*, 651−656.
(28) Christov, I. P.; Murnane, M. M.; Kapteyn, H. C. High-harmonic generation of attosecond pulses in the "single-cycle" regime. *Phys. Rev. Lett.* **1997**, *78*, 1251−1254.
(29) Goulielmakis, E.; Schultze, M.; Hofstetter, M.; Yakovlev, V. S.; Gagnon, J.; Uiberacker, M.; Aquila, A. L.; Gullikson, E. M.; Attwood, D. T.; Kienberger, R.; Krausz, F.; Kleineberg, U. Single-cycle nonlinear optics. *Science* **2008**, *320*, 1614−1617.
(30) Chini, M.; Zhao, K.; Chang, Z. The generation, characterization and applications of broadband isolated attosecond pulses. *Nat. Photonics* **2014**, *8*, 178−186.
(31) Hentschel, M.; Kienberger, R.; Spielmann, C.; Reider, G. A.; Milosevic, N.; Brabec, T.; Corkum, P.; Heinzmann, U.; Drescher, M.; Krausz, F. Attosecond metrology. *Nature* **2001**, *414*, 509−513.
(32) Wei, P.; Miao, J.; Zeng, Z.; Li, C.; Ge, X.; Li, R.; Xu, Z. Selective enhancement of a single harmonic emission in a driving laser field with subcycle waveform control. *Phys. Rev. Lett.* **2013**, *110*, 233903.
(33) Jin, C.; Wang, G.; Wei, H.; Le, A. T.; Lin, C. D. Waveforms for optimal sub-keV high-order harmonics with synthesized two- or three-colour laser fields. *Nat. Commun.* **2014**, *5*, 4003.
(34) Yang, Y.; Mainz, R. E.; Rossi, G. M.; Scheiba, F.; Silva-Toledo, M. A.; Keathley, P. D.; Cirmi, G.; Kärtner, F. X. Strong-field coherent control of isolated attosecond pulse generation. *Nat. Commun.* **2021**, *12*, 6641.
(35) Rossi, G. M.; Mainz, R. E.; Yang, Y.; Scheiba, F.; Silva-Toledo, M. A.; Chia, S. H.; Keathley, P. D.; Fang, S.; Mücke, O. D.; Manzoni, C.; Cerullo, G.; Cirmi, G.; Kärtner, F. X. Sub-cycle millijoule-level parametric waveform synthesizer for attosecond science. *Nat. Photonics* **2020**, *14*, 629−635.
(36) Travers, J. C.; Grigorova, T. F.; Brahms, C.; Belli, F. High-energy pulse self-compression and ultraviolet generation through soliton dynamics in hollow capillary fibres. *Nat. Photonics* **2019**, *13*, 547−554.
(37) Nisoli, M.; De Silvestri, S.; Svelto, O. Generation of high energy 10 fs pulses by a new pulse compression technique. *Appl. Phys. Lett.* **1996**, *68*, 2793−2795.
(38) Grigorova, T.; Brahms, C.; Belli, F.; Travers, J. C. Dispersion tuning of nonlinear optical pulse dynamics in gas-filled hollow capillary fibers. *Phys. Rev. A* **2023**, *107*, 063512.
(39) Voronin, A. A.; Zheltikov, A. M. Subcycle solitonic breathers. *Phys. Rev. A* **2014**, *90*, 043807.
(40) Brahms, C.; Belli, F.; Travers, J. C. Infrared attosecond field transients and UV to IR few-femtosecond pulses generated by high-energy soliton self-compression. *Phys. Rev. Res.* **2020**, *2*, 043037.
(41) Galán, M. F.; Jarque, E. C.; San Roman, J. Optimization of pulse self-compression in hollow capillary fibers using decreasing pressure gradients. *Opt. Express* **2022**, *30*, 6755−6767.
(42) Galán, M. F.; Jarque, E. C.; San Roman, J. Scalable sub-cycle pulse generation by soliton self-compression in hollow capillary fibers with a decreasing pressure gradient. *J. Eur. Opt. Society-Rapid Publ.* **2023**, *19*, 15.
(43) Brahms, C.; Austin, D. R.; Tani, F.; Johnson, A. S.; Garratt, D.; Travers, J. C.; Tisch, J. W. G.; Russell, P. S. J.; Marangos, J. P. Direct characterization of tuneable few-femtosecond dispersive-wave pulses in the deep UV. *Opt. Lett.* **2019**, *44*, 731−734.
(44) Brahms, C.; Belli, F.; Travers, J. C. Resonant dispersive wave emission in hollow capillary fibers filled with pressure gradients. *Opt. Lett.* **2020**, *45*, 4456−4459.
(45) Stammer, P.; Rivera-Dean, J.; Lamprou, T.; Pisanty, E.; Ciappina, M. F.; Tzallas, P.; Lewenstein, M. High photon number entangled states and coherent state superposition from the extreme ultraviolet to the far infrared. *Phys. Rev. Lett.* **2022**, *128*, 123603.
(46) Gorlach, A.; Tzur, M. E.; Birk, M.; Krüger, M.; Rivera, N.; Cohen, O.; Kaminer, I. High-harmonic generation driven by quantum light. *Nat. Phys.* **2023**, *19*, 1689−1696.
(47) Suda, A.; Hatayama, M.; Nagasaka, K.; Midorikawa, K. Generation of sub-10-fs, 5-mJ-optical pulses using a hollow fiber with a pressure gradient. *Appl. Phys. Lett.* **2005**, *86*, 111116.
(48) Jarque, E. C.; San Roman, J.; Silva, F.; Romero, R.; Holgado, W.; Gonzalez-Galicia, M. A.; Alonso, B.; Sola, Í. J.; Crespo, H. Universal route to optimal few-to single-cycle pulse generation in hollow-core fiber compressors. *Sci. Rep.* **2018**, *8*, 2256.
(49) Crego, A.; San Roman, J.; Jarque, E. C. Tools for numerical modelling of nonlinear propagation in hollow capillary fibres and their application. *J. Opt.* **2023**, *25*, 024005.
(50) Agrawal, G. P. *Nonlinear Fiber Optics*, 6th ed.; Academic Press, 2019.
(51) Marcatili, E. A. J.; Schmeltzer, R. A. Hollow metallic and dielectric waveguides for long distance optical transmission and lasers. *Bell Syst. Technol. J.* **1964**, *43*, 1783−1809.
(52) Nurhuda, M.; Suda, A.; Midorikawa, K.; Hatayama, M.; Nagasaka, K. Propagation dynamics of femtosecond laser pulses in a hollow fiber filled with argon: constant gas pressure versus differential gas pressure. *J. Opt. Soc. Am. B* **2003**, *20*, 2002−2011.
(53) Couairon, A.; Brambilla, E.; Corti, T.; Majus, D.; Ramírez-Góngora, O. J.; Kolesik, M. Practitioner's guide to laser pulse propagation models and simulation. *Eur. Phys. J. Spec. Top.* **2011**, *199*, 5−76.

https://doi.org/10.1021/acsphotonics.3c01897
ACS Photonics 2024, 11, 1673−1683

(54) Kaplan, A. E. Diffraction-induced transformation of near-cycle and subcycle pulses. *J. Opt. Soc. Am. B* **1998**, *15*, 951−956.
(55) Hernández-García, C.; Pérez-Hernández, J. A.; Ramos, J.; Jarque, E. C.; Roso, L.; Plaja, L. High-order harmonic propagation in gases within the discrete dipole approximation. *Phys. Rev. A* **2010**, *82*, 033432.
(56) Voronin, A. A.; Zheltikov, A. M. Soliton-number analysis of soliton-effect pulse compression to single-cycle pulse widths. *Phys. Rev. A* **2008**, *78*, 063834.
(57) Travers, J. C.; Chang, W.; Nold, J.; Joly, N. Y.; Russell, P. S. J. Ultrafast nonlinear optics in gas-filled hollow-core photonic crystal fibers. *J. Opt. Soc. Am. B* **2011**, *28*, A11−A26.
(58) Chen, C.-M.; Kelley, P. L. Nonlinear pulse compression in optical fibers: scaling laws and numerical analysis. *J. Opt. Soc. Am. B* **2002**, *19*, 1961−1967.
(59) Paulus, G. G.; Grasbon, F.; Walther, H.; Villoresi, P.; Nisoli, M.; Stagira, S.; Priori, E.; De Silvestri, S. Absolute-phase phenomena in photoionization with few-cycle laser pulses. *Nature* **2001**, *414*, 182−184.
(60) Zherebtsov, S.; et al. Carrier-envelope phase-tagged imaging of the controlled electron acceleration from SiO_2 nanospheres in intense few-cycle laser fields. *New J. Phys.* **2012**, *14*, 075010.
(61) Nisoli, M.; Sansone, G.; Stagira, S.; De Silvestri, S.; Vozzi, C.; Pascolini, M.; Poletto, L.; Villoresi, P.; Tondello, G. Effects of carrier-envelope phase differences of few-optical-cycle light pulses in single-shot high-order-harmonic spectra. *Phys. Rev. Lett.* **2003**, *91*, 213905.
(62) Borot, A.; Malvache, A.; Chen, X.; Jullien, A.; Geindre, J.-P.; Audebert, P.; Mourou, G.; Quéré, F.; Lopez-Martens, R. Attosecond control of collective electron motion in plasmas. *Nat. Phys.* **2012**, *8*, 416−421.
(63) Rudawski, P.; Harth, A.; Guo, C.; Lorek, E.; Miranda, M.; Heyl, C. M.; Larsen, E. W.; Ahrens, J.; Prochnow, O.; Binhammer, T.; Morgner, U.; Mauritsson, J.; L'Huillier, A.; Arnold, C. L. Carrier-envelope phase dependent high-order harmonic generation with a high-repetition rate OPCPA-system. *Eur. Phys. J. D* **2015**, *69*, 70.
(64) Hernández-García, C.; Holgado, W.; Plaja, L.; Alonso, B.; Silva, F.; Miranda, M.; Crespo, H.; Sola, I. J. Carrier-envelope-phase insensitivity in high-order harmonic generation driven by few-cycle laser pulses. *Opt. Express* **2015**, *23*, 21497−21508.
(65) Salières, P.; L'Huillier, A.; Lewenstein, M. Coherence control of high-order harmonics. *Phys. Rev. Lett.* **1995**, *74*, 3776−3779.
(66) Rundquist, A.; Durfee, C. G.; Chang, Z.; Herne, C.; Backus, S.; Murnane, M. M.; Kapteyn, H. C. Phase-matched generation of coherent soft X-rays. *Science* **1998**, *280*, 1412−1415.
(67) Gaarde, M. B.; Tate, J. L.; Schafer, K. J. Macroscopic aspects of attosecond pulse generation. *J. Phys. B* **2008**, *41*, 132001.
(68) Hernández-García, C.; Sola, I. J.; Plaja, L. Signature of the transversal coherence length in high-order harmonic generation. *Phys. Rev. A* **2013**, *88*, 043848.
(69) Weissenbilder, R.; Carlström, S.; Rego, L.; Guo, C.; Heyl, C. M.; Smorenburg, P.; Constant, E.; Arnold, C. L.; L'Huillier, A. How to optimize high-order harmonic generation in gases. *Nat. Rev. Phys.* **2022**, *4*, 713−722.
(70) Wikmark, H.; Guo, C.; Vogelsang, J.; Smorenburg, P. W.; Coudert-Alteirac, H.; Lahl, J.; Peschel, J.; Rudawski, P.; Dacasa, H.; Carlström, S.; Maclot, S.; Gaarde, M. B.; Johnsson, P.; Arnold, C. L.; L'Huillier, A. Spatiotemporal coupling of attosecond pulses. *Proc. Natl. Acad. Sci. U.S.A.* **2019**, *116*, 4779−4787.
(71) Quintard, L.; Strelkov, V.; Vabek, J.; Hort, O.; Dubrouil, A.; Descamps, D.; Burgy, F.; Péjot, C.; Mével, E.; Catoire, F.; Constant, E. Optics-less focusing of XUV high-order harmonics. *Sci. Adv.* **2019**, *5*, No. eaau7175.
(72) Rego, L.; Brooks, N. J.; Nguyen, Q. L. D.; San Roman, J.; Binnie, I.; Plaja, L.; Kapteyn, H. C.; Murnane, M. M.; Hernández-García, C. Necklace-structured high-harmonic generation for low-divergence, soft X-ray harmonic combs with tunable line spacing. *Sci. Adv.* **2022**, *8*, No. eabj7380.
(73) Serebryannikov, E. E.; von der Linde, D.; Zheltikov, A. M. Broadband dynamic phase matching of high-order harmonic generation by a high-peak-power soliton pump field in a gas-filled hollow photonic-crystal fiber. *Opt. Lett.* **2008**, *33*, 977−979.
(74) Heckl, O.; Baer, C.; Kränkel, C.; Marchese, S.; Schapper, F.; Holler, M.; Südmeyer, T.; Robinson, J.; Tisch, J.; Couny, F.; Light, P.; Benabid, F.; Keller, U. High harmonic generation in a gas-filled hollow-core photonic crystal fiber. *Appl. Phys. B: Laser Opt.* **2009**, *97*, 369−373.
(75) Gebhardt, M.; Heuermann, T.; Klas, R.; Liu, C.; Kirsche, A.; Lenski, M.; Wang, Z.; Gaida, C.; Antonio-Lopez, J. E.; Schülzgen, A.; Amezcua-Correa, R.; Rothhardt, J.; Limpert, J. Bright, high-repetition-rate water window soft X-ray source enabled by nonlinear pulse self-compression in an antiresonant hollow-core fibre. *Light Sci. Appl.* **2021**, *10*, 36.
(76) Crego, A.; Jarque, E. C.; San Roman, J. Influence of the spatial confinement on the self-focusing of ultrashort pulses in hollow-core fibers. *Sci. Rep.* **2019**, *9*, 9546.
(77) Chen, M.-C.; Arpin, P.; Popmintchev, T.; Gerrity, M.; Zhang, B.; Seaberg, M.; Popmintchev, D.; Murnane, M. M.; Kapteyn, H. C. Bright, coherent, ultrafast soft X-ray harmonics spanning the water window from a tabletop light source. *Phys. Rev. Lett.* **2010**, *105*, 173901.
(78) Teichmann, S. M.; Silva, F.; Cousin, S. L.; Hemmer, M.; Biegert, J. 0.5-keV soft X-ray attosecond continua. *Nat. Commun.* **2016**, *7*, 11493.
(79) Johnson, A. S.; Austin, D. R.; Wood, D. A.; Brahms, C.; Gregory, A.; Holzner, K. B.; Jarosch, S.; Larsen, E. W.; Parker, S.; Strüber, C. S.; Ye, P.; Tisch, J. W. G.; Marangos, J. P. High-flux soft X-ray harmonic generation from ionization-shaped few-cycle laser pulses. *Sci. Adv.* **2018**, *4*, No. eaar3761.
(80) Becker, A.; Plaja, L.; Moreno, P.; Nurhuda, M.; Faisal, F. H. M. Total ionization rates and ion yields of atoms at nonperturbative laser intensities. *Phys. Rev. A* **2001**, *64*, 023408.

https://doi.org/10.1021/acsphotonics.3c01897
ACS Photonics 2024, 11, 1673−1683